

1 **Ensemble streamflow forecasting over a cascade reservoir catchment with**
2 **integrated hydrometeorological modeling and machine learning**

3

4 Junjiang Liu¹, Xing Yuan^{1,2*}, Junhan Zeng¹, Yang Jiao¹, Yong Li³, Lihua Zhong³, Ling

5

Yao⁴

6

7 ¹School of Hydrology and Water Resources, Nanjing University of Information

8

Science and Technology, Nanjing 210044, China

9 ²Key Laboratory of Regional Climate-Environment for Temperate East Asia, Institute

10 of Atmospheric Physics, Chinese Academy of Sciences, Beijing 100029, China

11 ³Guangxi Meteorological Disaster Prevention Center, Nanning 530022, China

12 ⁴Guangxi Guiguan Electric Power Co., Ltd., Nanning 530029, China

13

14

15

16 *Hydrology and Earth System Sciences*

17 October 12, 2021

18

*Corresponding author address: Xing Yuan, School of Hydrology and Water Resources, Nanjing University of Information Science and Technology, Nanjing 210044, China E-mail: xyuan@nuist.edu.cn

19 **Abstract.** A popular way to forecast streamflow is to use bias-corrected
20 meteorological forecast to drive a calibrated hydrological model, but these
21 hydrometeorological approaches have deficiency over small catchments due to
22 uncertainty in meteorological forecasts and errors from hydrological models,
23 especially over catchments that are regulated by dams and reservoirs. For a cascade
24 reservoir catchment, the discharge of the upstream reservoir contributes to an
25 important part of the streamflow over the downstream areas, which makes it
26 tremendously hard to explore the added value of meteorological forecasts. Here, we
27 integrate the meteorological forecast, land surface hydrological model simulation and
28 machine learning to forecast hourly streamflow over the Yantan catchment, where the
29 streamflow is influenced both by the upstream reservoir water release and the
30 rainfall-runoff processes within the catchment. Evaluation of the hourly streamflow
31 hindcasts during the rainy seasons of 2013-2017 shows that the hydrometeorological
32 ensemble forecast approach reduces probabilistic [and deterministic](#) forecast errors by
33 ~~106%~~ ~~and deterministic forecast error by 6%~~ as compared with the traditional
34 ensemble streamflow prediction (ESP) approach during the first 7 days. The
35 deterministic forecast error can be further reduced by 6% in the first 72 hours when
36 combining the hydrometeorological forecast with the long short-term memory (LSTM)
37 deep learning method. However, the forecast skill for LSTM using only historical
38 observations drops sharply after the first 24 hours. This study implies the potential of
39 improving flood forecast over a cascade reservoir catchment by integrating
40 meteorological forecast, hydrological modeling and machine learning.

41 **Keywords:** Streamflow; Hydrological modeling; LSTM; Reservoir; Ensemble

42 forecast

43

44 **1. Introduction**

45 Flood events are the most destructive ones among the natural disasters, causing
46 huge damages to human society. Reservoirs are massively constructed to regulate
47 river flows, which has significantly reduced flood risks or damages (Ji et al., 2020).
48 However, the number and intensity of precipitation extreme events are increasing in
49 many areas as the global warming continues, thus amplify the potential of flood
50 hazards (Hao et al., 2013; Shao et al., 2016; Wei et al., 2018; Yuan et al., 2018a;
51 Wang et al., 2019). Accurate streamflow forecast is thus needed to provide guidelines
52 for reservoir operations (Robertson et al., 2013), especially when the flood risk is
53 increasing under global warming.

54 A common approach of streamflow forecast is to use hydrological models, where
55 the first attempt could be traced back to 1850s, using simple regression-type
56 approaches to predict discharge from observed precipitation (Mulvaney, 1850). Since
57 then, model concepts have been further augmented by designing new data networks,
58 addressing heterogeneity of hydrological processes, capturing the nonlinear
59 characteristics of hydrologic system and parameterizing models (Hornberger and
60 Boyer, 1995; Kirchner, 2006). With the advancements of computer technology and
61 high-resolution observation, a well-parameterized hydrological model can simulate
62 streamflow with high accuracy (Kollet et al., 2010; Ye et al., 2014; Graaf et al., 2015;
63 Yuan et al., 2018b).

64 Streamflow simulations from hydrological models heavily rely on
65 meteorological forcing inputs, especially precipitation, which can be measured at
66 in-situ gauges or retrieved from satellites and radars. However, for medium-range (2–
67 15 days ahead) streamflow forecasts, precipitation forecast is needed (Hopson et al.,
68 2002). To improve the forecast, ensemble techniques that can give a deterministic
69 estimate as well as its uncertainty became popular. Ensemble weather forecasting can
70 be traced back to 1963 when Leith transferred a deterministic forecast into an
71 ensemble using the Monte-Carlo method to describe the atmospheric uncertainty
72 (Leith, 1963). In the 1990s, ensemble forecasting was developed into an integral part
73 of numerical weather prediction, which showed higher skill than the deterministic
74 forecast even with higher model resolution (Toth et al., 2001). Due to its rapid
75 development, ensemble weather forecasts and climate predictions are applied to
76 hydrological forecasting studies by combining with hydrological models (Jasper et al.,
77 2002; Balint et al., 2006; Jaun et al., 2008; Xu et al., 2015; Yuan et al., 2016; Zhu et
78 al., 2019). Provided with streamflow variability, a reservoir can maintain a reliable
79 utility from natural streamflow better than provided with a deterministic streamflow
80 forecast (Zhao et al., 2011). However, the streamflow prediction skill depends on
81 whether the precipitation forecasts introduced into the hydrological model are skillful
82 (Alfieri et al., 2013). When assessing the skill of this hydrometeorological forecast
83 approach, a benchmark is needed. Using ensembles of historical climatology data
84 (Day, 1985) as meteorological forecast inputs, which is known as ensemble
85 streamflow prediction (ESP), is often selected as the benchmark approach.

86 Evaluations of hydrological forecasts indicated that forecast skill has a close
87 relationship with catchment size, geographical locations and resolutions (Alfieri et al.,
88 2013; Pappenberger et al., 2015), which means there is a necessity to compare with
89 the ESP to show the skill of the hydrometeorological forecast approach.

90 Although physically based hydrological models are widely used, it is still hard
91 to apply a hyper-resolution distributed model for streamflow forecasting due to its
92 demand for observation data, complex model structures and computational resources
93 requirements for calibration and application (Wood et al., 2011; Kratzert et al., 2018;
94 Yaseen et al., 2018). In cascade reservoir systems, there are two sources of streamflow,
95 one is from the rainfall within the interval basin and the other is from the upstream
96 reservoir discharge. While the rainfall-runoff relationship is well studied, it is
97 challenging to reproduce the reservoir operating rules in a physical model (Gao et al.,
98 2010; Zhang et al., 2016; Dang et al., 2020).

99 Machine learning methods can recognize patterns hidden in input data and can
100 simulate or predict streamflow without explicit descriptions of the underlying physical
101 processes (Kisi et al., 2007; Adnan et al., 2019). Neural networks are suitable for
102 streamflow forecasting among machine learning models, some of them can even
103 outperform physically based hydrological models. For example, Humphrey et al.
104 (2016) showed that their combined Bayesian artificial neural network with [the modèle](#)
105 [du Génie Rural à 4 paramètres Journalier \(GR4J\) modèle](#) approach outperforms the
106 GR4J model in monthly streamflow forecasting. Kratzert et al. (2019) showed that the

107 long short-term memory (LSTM)-based approach outperforms a well-calibrated
108 Sacramento Soil Moisture Accounting Model (SAC-SMA). Yang et al. (2020) used
109 the geomorphology-based hydrological model (GBHM) combined with traditional
110 ANN model to simulate daily streamflow, which can provide enough physical
111 evidence and can run with less observation data. Although neural network models are
112 criticized with little physical evidence (Abrahart et al., 2012), their potential in
113 hydrological forecasting is yet to be explored.

114 In this study, we combine the machine learning with hydrometeorological
115 approach for hourly streamflow forecast over a ~~data limited~~ cascade reservoir
116 catchment located in southwestern China. We use the meteorological hindcast data
117 from European Centre for Medium-Range Weather Forecasts (ECMWF) model that
118 participated in the THORPEX Interactive Grand Global Ensemble (TIGGE) project to
119 drive a newly developed high-resolution land surface model, named as the
120 Conjunctive Surface-Subsurface Process model version 2 (CSSPv2, Yuan et al.,
121 2018b).~~We use the TIGGE-ECMWF meteorological forecasts to drive a newly~~
122 ~~developed CSSPv2 high-resolution land surface model (Yuan et al., 2018)~~ to provide
123 runoff and streamflow forecasts, and correct the forecasts via LSTM model. We aim
124 to improving flood forecast over the cascade reservoir catchment by integrating
125 meteorological forecast, hydrological modeling and machine learning.~~and adjust the~~
126 ~~results via LSTM model to improve streamflow forecast. We~~ So we strive to (1)
127 calibrate the hydrological model, (2) bias correct the meteorological forecasts, (3)

128 evaluate the streamflow forecast skill and (4) test the physical-statistical combined
129 approach.

130 **2. Study Area, Data, Model and Method**

131 *2.1 Study Area*

132 The Yantan Hydropower Station is in the middle reaches of Hongshui River in
133 Dahua Yao Autonomous County, Guangxi Province. The Yantan Hydropower Station
134 is the fifth level in the 10-level development of Hongshuihe hydropower base in
135 Nanpanjiang River, connected with upstream Longtan Hydropower Station and the
136 downstream Dahua Hydropower Station. The drainage area between the Longtan
137 Hydropower Station and Yantan Hydropower Station is 8,900 km². The annual mean
138 streamflow at Yantan gauge is 55.5 billion m³. The river passes through karst
139 mountain area, with narrow valley, steep slope and scattered cultivated land, and the
140 average slope is 0.036%. Figure 1 shows the locations of 4 hydrological gauges, with
141 detailed information listed in Table 1.

142 *2.2 Data and Method*

143 *2.2.1 Hydrometeorological observations*

144 There are 97 meteorological observation stations within the catchment (Figure
145 1). Here, observed hourly 2m-temperature, 10m-wind speed, relative humidity,
146 accumulated precipitation and surface pressure data were interpolated into a 5km
147 gridded observation dataset via inverse distance weight method. The hourly surface

148 downward solar radiation data from China Meteorological Administration Land Data
149 Assimilation System (CLDAS) was also interpolated into 5km via bilinear
150 interpolation method. The hourly surface downward thermal radiation (long) was
151 estimated by specific humidity, pressure, temperature. This dataset was used to drive
152 the CSSPv2 land surface hydrological model.

153 The monthly runoff for each 5km grid was estimated by disaggregating control
154 streamflow station observations with the ratio of observed grid monthly precipitation
155 and catchment mean precipitation. The gridded runoff was used to calibrate the
156 CSSPv2 model at each grid (Yuan et al., 2016)-, which would generate distributed
157 model parameters that are different within the catchment to better represent the
158 heterogeneity of the rainfall-runoff processes.

159 2.2.2 Ensemble Meteorological hindcast data and ESP hindcasts

160 The TIGGE dataset consists of ensemble forecast data from 10 global Numerical
161 Weather Prediction centers started from October 2006, which has been made available
162 for scientific research, via data archive portals at ECMWF and the China
163 Meteorological Administration (CMA). TIGGE has become a focal point for a range
164 of research projects, including research on ensemble forecasting, predictability, and
165 the development of products to improve the prediction of severe weather (Bougeault
166 et al., 2010). In this paper, TIGGE data from April to September during 2013-2017
167 from ECMWF were used as meteorological hindcast data. The 3-hourly
168 meteorological hindcasts for 7-day lead time from 51 ensemble members (including

169 control forecast) were interpolated into 5km resolution via bilinear interpolation. The
170 forecast precipitation and temperature were corrected to match the observational
171 means to remove the biases.

172 The ESP was accomplished by applying historical meteorological forcings (Day,
173 1985). In this paper, the meteorological forcings from the same date as the forecast
174 start date to the next 9 days of each year (excluding the target year) were selected as
175 the ESP forcings. Take April 1st, 2013 as example, the 7-day observations started from
176 April 1st to April 10th (i.e., April 1st-April 7th, April 2nd-April 8th, ..., April 10th-April
177 16th) in the year of 2014, 2015, 2016 and 2017 were selected as the forecast ensemble
178 forcings of the issue date (April 1st), with a total of 40 ensemble members. [The](#)
179 [detailed information about the raw datasets are listed in Table 2](#)

180 2.2.3 CSSPv2 streamflow hindcasts

181 The physical hydrological model used in this paper is the Conjunctive
182 Surface-Subsurface Process model version 2 (CSSPv2; Yuan et al., 2018). The
183 CSSPv2 model is a distributed, grid-based land surface hydrological model, which
184 was developed from the Common Land Model (Dai et al., 2003, 2004), but with better
185 representations in lateral surface and subsurface hydrological processes and their
186 interactions. The routing model used here employs the kinetic wave equation as
187 covariance function, which is solved via a Newton algorithm. A main reason for
188 adopting this covariance function is that it suits the basin with mountainous terrain.
189 The CSSPv2 model was successfully used to perform a high-resolution (3 km) land

190 surface simulation over the Sanjiangyuan region, which is the headwater of major
191 Chinese rivers (Ji and Yuan, 2018). In this paper, we calibrated CSSPv2 model against
192 monthly estimated runoff to simulate the natural hydrological processes by using the
193 Shuffled Complex Evolution (SCE-UA) approach (Duan et al., 1994). The calibrated
194 parameters include maximum velocity of baseflow, variable infiltration curve
195 parameter, fraction of maximum soil moisture where non-linear baseflow occurs and
196 fraction of maximum velocity of baseflow where non-linear baseflow begins. The
197 hourly observed streamflow at Yantan hydrological gauge was used to calibrate the
198 CSSPv2 routing model manually, including slope, river density, roughness, width and
199 depth. The observed streamflow at Longtan hydrological gauge were added into the
200 corresponding grid to provide upstream streamflow information. We used a
201 high-resolution elevation database (hereafter referred to as DEM30) for sub-grid
202 parameterization and figured out the initial values of these river channel parameters.
203 We first extracted the slope angle and the natural river flow path from DEM30, and
204 then identified the accurate river network using a drainage area threshold of 0.18 km².
205 River density and bed slope values for each 5km grid were calculated as:

$$206 \quad \underline{\underline{rivden = \sum l / A,}} \quad (1)$$

$$207 \quad \underline{\underline{bedslp = mean(\tan(\beta)),}} \quad (2)$$

208 where rivden is the river density (km/km²), bedslp is the river channel bed slope
209 (unitless), A is the area of a 5km grid (km²), $\sum l$ is the total river channel length (m)
210 within the grid, β is the slope angle (radian) for each river segment located in the grid.

211 Other river channel parameters were estimated by empirical formulas (Getirana
212 et al., 2012; Luo et al., 2017) as follows:

$$213 \quad \underline{W = 1.956 \times A_{acc}^{0.413},} \quad (3)$$

$$214 \quad \underline{H = 0.245 \times A_{acc}^{0.342},} \quad (4)$$

$$215 \quad \underline{n = 0.03 + (0.05 - 0.03) \frac{H_{max} - H}{H_{max} - H_{min}},} \quad (5)$$

216 where W, H and n are river width (m), depth (m) and roughness (unitless) for each
217 5km grid; Aacc means the upstream drainage area (km²); Hmax and Hmin refer to the
218 maximum and minimum values of river depth calculated by Eq. (4).

219 Through a trial-and-error procedure, we calibrated these river channel parameters
220 to match the simulated streamflow with observed hourly records at Yantan
221 hydrological gauge. The simulation results were evaluated by calculating the
222 Nash-Sutcliffe efficiency (NSE) with corresponding observation data. The
223 descriptions of the calibrated parameters and their range are listed in Table 3

224 ~~The simulation results were evaluated by calculating the Nash-Sutcliffe~~
225 ~~efficiency (NSE) with corresponding observation data.~~

226 After calibration, we drove the CSSPv2 model using 5km regridded and
227 bias-corrected TIGGE-ECMWF forecast forcing during 2013-2017 to provide a set of
228 7-day hindcasts ~~(Figure 2)~~. Streamflow hindcasts both from the ESP and the
229 hydrometeorological approach (TIGGE-ECMWF/CSSPv2) were corrected by

230 matching monthly mean streamflow observations to remove the biases, and the
231 hindcast experiments were termed as ESP-Hydro and Meteo-Hydro (Table 42). Figure
232 2 shows the procession of the CSSPv2 hindcasts: the calibrated CSSPv2 model was
233 first driven with observation dataset to generate initial hydrological conditions (soil
234 moisture, surface water, etc.) for each forecast issue date, then CSSPv2 model was
235 driven with forecast data (TIGGE-ECMWF or ESP) at every forecast issue date with
236 the generated initial conditions to perform a 7-day hindcast.

237 2.2.4 LSTM streamflow forecast

238 LSTM is a type of recurrent neural network model which learns from sequential
239 data. The input of the LSTM model includes forecast interval streamflow at the
240 specified forecast step obtained from TIGGE-ECMWF/CSSPv2, historical upstream
241 streamflow observation, and historical streamflow observation at Yantan hydrological
242 gauge. The network was trained on sequences of April to September in 2013-2017,
243 with six historical streamflow observations and one forecast interval streamflow to
244 predict the total streamflow at each forecast time step (Figure 2). The LSTM was
245 calibrated through a cross validation method, by leaving the target year out.

246 Before calibration, all input and output variables were normalized as follows:

$$247 \quad \mathbf{q}_0 = \frac{(\mathbf{q} - \mathbf{q}_{\min})}{(\mathbf{q}_{\max} - \mathbf{q}_{\min})}, \quad (67)$$

248 Where \mathbf{q}_0 , \mathbf{q} , \mathbf{q}_{\max} and \mathbf{q}_{\min} are the normalized variable, input variable, the
249 maximum and minimum of the sequence of the variable. The hindcast experiment was

250 termed as Meteo-Hydro-LSTM (Table 2). In addition, we also tried an LSTM
 251 streamflow forecast approach which only uses 6-hr historical streamflow data as
 252 inputs, and the experiment was termed as LSTM (Table 2). The process of LSTM is
 253 similar to Meteo-Hydro-LSTM but without the forecast interval streamflow, which is
 254 also shown in Figure 2.

255 2.3 Evaluation Method

256 The root-mean squared error (RMSE) was used to evaluate the deterministic
 257 forecast, i.e., the ensemble means of 51 (ECMWF) or 40 (ESP) forecast members. To
 258 evaluate probabilistic forecasts, the Continuous Ranked Probability Score (CRPS)
 259 was calculated as follows:

$$260 \quad CRPS = \int_{-\infty}^{\infty} [F(y) - F_o(y)]^2, \quad (71)$$

261 where

$$262 \quad F_o(y) = \begin{cases} 0, & y < \text{observed value} \\ 1, & y \geq \text{observed value} \end{cases} \quad (82)$$

263 is a cumulative-probability step function that jumps from 0 to 1 at the point where the
 264 forecast variable y equals the observation and $F(y)$ is a cumulative-probability
 265 distribution curve formed by the forecast ensembles. The CRPS has a negative
 266 orientation (smaller values are better), and it rewards concentration of probability
 267 around the step function located at the observed value (Wilks, 2005). The skill score
 268 for deterministic forecast was calculated as

269
$$SS_{RMSE} = \frac{RMSE - RMSE_{ref}}{0 - RMSE_{ref}} = 1 - \frac{RMSE}{RMSE_{ref}} \quad (93)$$

270 The skill score for probabilistic forecast (CRPSS) could be calculated similarly based
271 the CRPS.

272 3. Results

273 3.1 Evaluation of CSSP calibration

274 The employed CSSPv2 model is a fully distributed hydrological model and the
275 streamflow is calculated through a process of converting gridded rainfall into runoff
276 and a process of runoff routing. Figure 3 shows the runoff calibration results by
277 calculating the NSE of monthly runoff simulations compared with observed gridded
278 monthly runoff. After calibrating the CSSPv2 runoff model, the NSE of all grids are
279 above 0, which indicates that the runoff simulation results in all grids are more
280 reliable than the climatology method. In addition, grids distributed in the downstream
281 region have better NSE than the upstream grids. The NSE values of the grids in the
282 southern part are greater than 0.5, which accounts for two thirds of the interval basin
283 area. Higher NSE in the upstream part of Jiazhuan station (Figure 1) is due to more
284 humid climate (not shown), where hydrological models usually have better
285 performance over wetter areas. For the downstream areas with less precipitation, the
286 higher NSE is related to the higher percentage of sand in the soil (not shown). Under
287 the same meteorological conditions, there is higher hydraulic conductivity with higher
288 sand content (Wang et al., 2016), and it yields less runoff under infiltration excess.

289 [which is more suitable for the saturation excess-based runoff generation for the](#)
290 [CSSPv2 model \(Yuan et al., 2018b\).](#)

291 Figures 4 and 5 show the results after the calibration of the routing model, where
292 ~~CSSPv2 is driven by observed meteorological forcings to provide streamflow~~
293 ~~simulations and compare against~~ ~~time series of CSSPv2 simulated streamflow are~~
294 ~~compared against~~ observed streamflow at Yantan hydrological gauge. Figure 4 shows
295 the daily and monthly streamflow simulation results. The monthly result (Fig. 4f)
296 shows that the simulated streamflow closely follows the observed streamflow, and the
297 NSE is 0.96. The daily streamflow simulations during flood seasons (Figs. 4a-4e) also
298 show a good performance, and the NSE is 0.92. During June and July in years of 2014,
299 2015 and 2017, the CSSPv2 model underestimated the daily streamflow with a
300 maximum of 1104 m³/s and an average of 334 m³/s (Figs. 4b, 4c, 4e). In years of 2013
301 and 2016, the difference between observed and simulated streamflow is relatively
302 small, and the average difference is 96 m³/s (Figs. 4a, 4d).

303 Figure 5 shows the hourly streamflow simulation results for a few flood events.
304 Figure 5a shows that the CSSPv2 model can accurately simulate the streamflow
305 response to a rainfall event after a dry period. Figures 5b-5d show that for
306 instantaneous heavy rainfall events, the CSSPv2 model over-predicted the water loss
307 during recession period. Figures 5e-5f show that for continuous rainfall events, the
308 simulated streamflow has a larger fluctuation than observation. The simulated
309 streamflow is also smoother than observation. Nevertheless, the NSE for the hourly

310 streamflow simulation is 0.61, which suggests that CSSPv2 has an acceptable
311 performance at hourly time scale.

312 *3.2 Bias correction of TIGGE-ECMWF meteorological forecasts*

313 The resolution of TIGGE-ECMWF grid data is 0.25° , so the data was
314 interpolated to 5km grid to drive the CSSPv2 model. We calculated both observations'
315 and TIGGE-ECMWF's yearly average precipitation and temperature, then performed
316 a bias correction by adding back the difference (for temperature) or multiplying back
317 the ratio (for temperature) to match the observations' averages. Figure 6 shows the
318 correlation coefficient and RMSE of TIGGE-ECMWF precipitation and temperature
319 forecasts as compared against observations, either before or after bias correction. The
320 51-ensemble mean precipitation and temperature (the red dashed lines) shows better
321 performance than the best ensemble members (the green dashed lines), with an
322 average RMSE reduction of 3.66 mm/day and average correlation increase of 0.04 for
323 precipitation, and average RMSE reduction of 0.1K and average correlation increase
324 of 0.03 for temperature. After bias correction, the 51-ensemble means still perform
325 better than best ensemble members. Compared with ensemble mean results before
326 bias correction, the RMSE reduced by 0.23 mm/day for the bias-corrected
327 precipitation, and reduced by 1K for the bias-corrected surface air temperature. For
328 the bias-corrected ensemble mean results, the average RMSE and correlation are 14.6
329 mm/day and 0.44 for precipitation, and 1.25 K and 0.87 for surface air temperature.

330 *3.3 Comparison between ESP-Hydro and Meteo-Hydro streamflow forecast*

331 Figure 7 presents the variations of RMSE and CRPS for ESP-Hydro and

332 Meteo-Hydro hourly streamflow forecast at Yantan hydrological gauge. For
333 probabilistic forecast, Figure 7a shows that the CRPS for Meteo-Hydro streamflow
334 forecast ranges from ~~160-165~~ to ~~230-225~~ m^3/s while the CRPS for ESP-Hydro
335 streamflow forecast ranges from ~~160-170~~ to ~~240~~~~230~~ m^3/s . The Meteo-Hydro approach
336 performs better than ESP-Hydro with lower CRPS at all lead times, with an average
337 of ~~10~~6% improvement in CRPSS (Figure 7c). For deterministic forecast, Figure 7b
338 shows that the RMSE for Meteo-Hydro streamflow forecast ranges from 250 to 350
339 m^3/s , while the RMSE for ESP-Hydro streamflow forecast ranges from 250 to 390
340 m^3/s . The Meteo-Hydro approach also performs better than ESP-Hydro with lower
341 RMSE at all lead times especially after 3 days, with the average reduction of RMSE
342 reaching 6% (Figure 7d).

343 Figure 7 also shows that both forecast skills have a similar diurnal cycle, where
344 RMSE and CRPS reach their peaks around 00UTC and drop to their lows at 06UTC.
345 Figure 8 shows the diurnal cycle of model employed variables, which are observed
346 catchment mean rainfall, observed streamflow at Yantan and Longtan hydrological
347 gauges, to explain the diurnal cycle of ESP-Hydro and Meteo-Hydro forecasting skills.
348 These three input variables show different diurnal patterns. The observed rainfall
349 starts to rise at 00UTC and reaches its maximum at 06UTC. The observed streamflow
350 at Yantan hydrological gauge drops to its minimum at 12UTC and rises to its
351 maximum at 00UTC. The streamflow from upstream Longtan hydrological gauge
352 starts to drop at 00UTC and reaches its minimum at 06UTC. After comparing these
353 diurnal cycles with the cycle of forecast skill, it is found that the forecast skill

354 decreases when the upstream Longtan outflow starts to decrease, and the precipitation
355 starts to increase. When the upstream Longtan outflow increases and the precipitation
356 starts to decrease (after 06UTC), the forecast skill rises. Such information indicates
357 that the hydrological model performs worse in the case of heavier rainfall event, and
358 the decrease of upstream outflow may amplify such degradation when the portion of
359 interval rainfall-runoff increased.

360 *3.4 Meteo-Hydro-LSTM streamflow forecast*

361 Machine learning methods can recognize patterns hidden in input data and can
362 simulate or predict streamflow without explicit descriptions of the underlying physical
363 processes. Figure 9 shows the RMSE of Meteo-Hydro-LSTM streamflow forecast
364 using the ensemble mean hydrological forecast as described in the section above, and
365 the past 6-hour observed streamflow of Yantan hydrological gauge as input.
366 Compared with Meteo-Hydro and ESP-Hydro approach, applying LSTM model can
367 further decrease the RMSE within the first 72 hours. The RMSE of
368 Meteo-Hydro-LSTM approach ranges from 205 to 363 m³/s during these three days,
369 suggesting an average of 6% improvement against Meteo-Hydro approach.

370 Figure 9 also shows the RMSE of LSTM streamflow forecast only using the past
371 6-hour observed streamflow of Yantan hydrological gauge as input. Without using the
372 physical model forecast, RMSE is improved only when the lead time is less than 1 day.
373 And the performance of LSTM is far worse than Meteo-Hydro streamflow forecast
374 when lead time is more than 2 days.

375 Figure 10 shows several examples of streamflow forecasts by
376 Meteo-Hydro-LSTM approach and Meteo-Hydro approaches to show the forecast
377 improvements in details. The Meteo-Hydro-LSTM approach reduced the flood peak
378 value and the water loss during flood recession period compared with Meteo-Hydro
379 streamflow forecast approach, which improves the streamflow prediction for most
380 cases (Figs. 10b-10f). However, when the upstream reservoir's flood operation is
381 triggered by continuous heavy rain, the Meteo-Hydro may underpredict the
382 streamflow. With the LSTM model further decreases the streamflow, the
383 Meteo-Hydro-LSTM method can end up with worsening the streamflow forecast,
384 which means the machine learning method may improve forecasts when trained in
385 different flood operating situations (Figure 10a).

386 **4. Conclusions**

387 In this study, we developed and evaluated a streamflow forecasting framework
388 by coupling meteorological forecasts with a land surface hydrological model (CSSPv2)
389 and a machine learning method (LSTM) over a cascade reservoir catchment using
390 hindcast data from 2013 to 2017. The monthly observed runoff was used to calibrate
391 the runoff generation module of the CSSPv2 model grid by grid, and the hourly
392 observed streamflow at Yantan hydrological gauge was used to calibrate the routing
393 module of the CSSPv2 model. Then, the bias-corrected TIGGE-ECMWF ensemble
394 forecasts were used to drive the CSSPv2 for streamflow forecasts, and the LSTM

395 model was used to correct the streamflow forecasts, resulted in an integrated
396 meteorological-hydrological-machine learning forecast framework.

397 With automatic offline calibration of the CSSPv2 model, and the NSE values are
398 0.96, 0.92 and 0.61 for streamflow simulations at the Yantan gauge at monthly, daily
399 and hourly time scales, respectively. The bias-corrected ensemble mean
400 TIGGE-ECMWF forcings which perform the best among all ensemble members,
401 show average RMSE and correlation of 14.6 mm/day and a 0.44 for precipitation
402 forecasts, and 1.3 K and 0.87 for surface air temperature forecasts. By comparing with
403 the hourly observed streamflow, the integrated hydrometeorological forecast approach
404 (Meteo-Hydro) increases the probabilistic and deterministic forecast skill against the
405 initial condition-based approach (ESP-Hydro) by ~~106%~~, ~~(CRPSS)~~ and ~~6%~~ ~~(RMSE~~
406 ~~skill score), respectively.~~

407 Adding LSTM model to the hydrometeorological forecast (Meteo-Hydro-LSTM)
408 can further reduce the forecast error. Within the first 72 hours, LSTM can improve the
409 forecast skill with a maximum of 25% and an average of 6%. However, if we do not
410 use the streamflow predicted by Meteo-Hydro, the error from the LSTM increases
411 rapidly after 24 hours, and the historical data-based LSTM method performs worse
412 than the Meteo-Hydro method.

413 Most cascade reservoirs yet cannot forecast streamflow beyond 6 hours, and the
414 integrated Meteo-Hydro-LSTM approach has potential to improve the forecasts at
415 long leads. This study mainly focused on exploring the added values of

416 meteorology-hydrology coupled forecast and LSTM forecast in a non-closed
417 catchment, so the forecast uncertainty from upstream outflow was ignored by using
418 the observed outflow. In the future, the upstream outflow forecast is planned to
419 include, but this requires the development of upstream hydrometeorological forecast
420 capability, as well as the reservoir regulation forecast that is very challenging. The
421 artificial intelligence (AI) techniques are expected to complement the physical model
422 for reservoir regulation forecast.

423

424 **Acknowledgement.** This work was supported by National Key R&D Program of
425 China (2018YFA0606002), National Natural Science Foundation of China
426 (41875105), and Natural Science Foundation of Jiangsu Province for Distinguished
427 Young Scholars (BK20211540).

428

429 **Data availability.** The TIGGE-ECMWF hindcast data can be downloaded from
430 <https://apps.ecmwf.int/datasets/data/tigge/levtype=sfc/type=pf/> (Parsons et al., 2017),
431 the in-situ observations and simulation data are available upon request.

432

433 **References**

- 434 Abrahart, R. J., Anctil, F., Coulibaly, P., Dawson, C. W., Mount, N. J., See, L. M., et
435 al.: Two decades of anarchy? emerging themes and outstanding challenges for
436 neural network river forecasting. *Prog. Phys. Geogr.* 36(4), 480-513.
437 <https://doi.org/10.1177/0309133312444943>, 2012.
- 438 Adnan, R.M., et al.: Daily streamflow prediction using optimally pruned extreme
439 learning machine. *J. Hydrol.* 577. <https://doi.org/10.1016/j.jhydrol.2019.123981>,
440 2019.
- 441 Alfieri, L., Burek, P., Dutra, E., Krzeminski, B., & Pappenberger, F.: GloFAS-global
442 ensemble streamflow forecasting and flood early warning. *Hydrol. Earth Syst.*
443 *Sci.* 17 (3), 1161–1175. <https://doi.org/10.5194/hess17-1161-2013>, 2013.
- 444 Balint, G., Csik, A., Bartha, P., Gauzer, B., Bonta, I.: Application of meteorological
445 ensembles for Danube flood forecasting and warning. In: Marsalek, J., Stancalie,
446 G., Balint, G. (Eds.), *Transboundary Floods: Reducing Risks through Flood*
447 *Management*. Springer, NATO Science Series, Dordrecht, The Netherlands, pp.
448 57–68. https://doi.org/10.1007/1-4020-4902-1_6, 2006.
- 449 Bougeault, P., et al.: The THORPEX interactive grand global ensemble, *Bull. Am.*
450 *Meteorol. Soc.*, 91, 1059–1072. <http://dx.doi.org/10.1175/2010BAMS2853.1>,
451 2010.
- 452 Dai, Y., Dickinson, R. E., Wang, Y. P.: A two-big-leaf model for canopy temperature,
453 photosynthesis, and stomatal conductance. *J. Clim.* 17(12),2281–2299.
454 [https://doi.org/10.1175/1520-0442\(2004\)017<2281:ATMFCT>2.0.CO;2](https://doi.org/10.1175/1520-0442(2004)017<2281:ATMFCT>2.0.CO;2), 2004.

455 Dai, Y., Zeng, X., Dickinson, R. E., Baker, I., Bonan, G. B., Bosilovich, M. G., et al.:
456 The Common Land Model. *Bull. Am. Meteorol. Soc.* 84(8), 1013–1024.
457 <https://doi.org/10.1175/BAMS-84-8-1013>, 2003.

458 Dang, T. D., Chowdhury, A. K., Galelli, S.: On the representation of water reservoir
459 storage and operations in large-scale hydrological models: implications on
460 model parameterization and climate change impact assessments. *Hydrol. Earth
461 Syst. Sci.*, 24, 397–416. <https://doi.org/10.5194/hess-24-397-2020>, 2020.

462 Day, G.N.: Extended Streamflow Forecasting Using NWSRFS. *J. Water Resour. Plan
463 Manag.* 111 (2): 157-170, 1985.

464 Duan, Q., Sorooshian, S., Gupta, V. K.: Optimal use of SCEUA global optimization
465 method for calibrating watershed models, *J. Hydrol.*, 158, 265–284,
466 [https://doi.org/10.1016/0022-1694\(94\)90057-4](https://doi.org/10.1016/0022-1694(94)90057-4), 1994.

467 Gao, X., Zeng, Y., Wang, J., Liu, H.: Immediate impacts of the second impoundment
468 on fish communities in the Three Gorges Reservoir, *Environ. Biol. Fish.*, 87,
469 163–173. <https://doi.org/10.1007/s10641-009-9577-1>, 2010.

470 [Getirana, A. C. V., Boone, A., Yamazaki, D., Decharme, B., Papa, F., and Mognard, N.:](#)
471 [The Hydrological Modeling and Analysis Platform \(HyMAP\): Evaluation in the](#)
472 [Amazon Basin, J. Hydrometeorol., 13, 1641–1665,](#)
473 [<https://doi.org/10.1175/JHM-D-12-021.1>, 2012.](#)

474 Graaf, I. D., Sutanudjaja, E. H., Beek, L. V., et al.: A high-resolution global-scale
475 groundwater model. *Hydrol. Earth Syst. Sci.* 19(2):823-837.
476 <https://doi.org/10.5194/hess-19-823-2015>, 2015.

477 Hao, Z., Aghakouchak, A., Phillips, T. J.: Changes in concurrent monthly precipitation
478 and temperature extremes. *Environ. Res. Lett.* 8(3), 1402-1416.
479 <https://doi.org/10.1088/1748-9326/8/3/034014>, 2013.

480 Hopson, T., Webster, P.: A 1–10 day ensemble forecasting scheme for the major river
481 basins of Bangladesh: forecasting severe floods of 2003–2007. *J. Hydrometeorol.*
482 11(3), 618-641. <https://doi.org/10.1175/2009JHM1006.1>, 2010.

483 Hornberger, G. M., E. W. Boyer.: Recent advances in watershed modeling, U.S. Natl.
484 Rep. Int. Union Geod. Geophys. 1991 – 1994, *Rev. Geophys.*, 33, 949 – 957.
485 <https://doi.org/10.1029/95RG00288>, 1995.

486 Humphrey, G.B., Gibbs, M.S., Dandy, G.C., Maier, H.R.: A hybrid approach to
487 monthly streamflow forecasting: Integrating hydrological model outputs into a
488 Bayesian artificial neural network. *J. Hydrol.* 540, 623–640.
489 <https://doi.org/10.1016/j.jhydrol.2016.06.026>, 2016.

490 Jasper, K., Gurtz, J., Lang, H.: Advanced flood forecasting in Alpine watersheds by
491 coupling meteorological observations and forecasts with a distributed
492 hydrological model. *J. Hydrol.* 267 (1–2), 40–52.
493 [https://doi.org/10.1016/S0022-1694\(02\)00138-5](https://doi.org/10.1016/S0022-1694(02)00138-5), 2002.

494 Jaun, S., Ahrens, B., Walser, A., Ewen, T., Schär, C.: A probabilistic view on
495 the August 2005 floods in the upper Rhine catchment. *Nat. Hazard Earth Sys.* 8,
496 281–291. <https://doi.org/10.5194/nhess-8-281-2008>, 2008.

497 Ji, P., X. Yuan., Y. Jiao., C. Wang., S. Han., C. Shi.: Anthropogenic contributions to
498 the 2018 extreme flooding over the upper Yellow River basin in China. *Bull. Am.*

499 Meteorol. Soc. 101(1), S89-S94, <https://doi.org/10.1175/BAMS-D-19-0105.1>,
500 2020.

501 Kirchner, J. W.: Getting the right answers for the right reasons: Linking measurements,
502 analyses, and models to advance the science of hydrology, *Water Resour. Res.*
503 42, 1–5. <https://doi.org/10.1029/2005WR004362>, 2006.

504 Kisi, O.: Streamflow forecasting using different artificial neural network algorithms. *J.*
505 *Hydrol. Eng.* 12 (5), 532–539.
506 [https://doi.org/10.1061/\(ASCE\)1084-0699\(2007\)12:5\(532\)](https://doi.org/10.1061/(ASCE)1084-0699(2007)12:5(532)), 2007.

507 Kollet, S. J., Maxwell, R. M., Woodward, C. S., Smith, S., Vanderborght, J., &
508 Vereecken, H., et al.: Proof of concept of regional scale hydrologic simulations
509 at hydrologic resolution utilizing massively parallel computer resources. *Water*
510 *Resour. Res.* 46(4). <https://doi.org/10.1029/2009WR008730>, 2010.

511 Kratzert, F., Klotz, D., Brenner, C., Schulz, K., Herrnegger, M.: Rainfall–runoff
512 modelling using long short-term memory (LSTM) networks. *Hydrol. Earth Syst.*
513 *Sci.* 22 (11), 6005–6022. <https://doi.org/10.5194/hess-22-6005-2018>, 2018.

514 Kratzert, F., Klotz, D., Herrnegger, M., Sampson, A. K., Hochreiter, S., Nearing, G. S.:
515 Towards Improved Predictions in Ungauged Basins: Exploiting the Power of
516 Machine Learning. *Water Resour. Res.* 55.
517 <https://doi.org/10.1029/2019wr026065>, 2019.

518 Leith, C. E.: Theoretical skill of monte carlo forecasts. *Mon. Weather Rev.* 102(6),
519 409-418. [https://doi.org/10.1175/1520-0493\(1974\)102:2.0.CO;2](https://doi.org/10.1175/1520-0493(1974)102:2.0.CO;2), 1974.

520 [Luo, X., Li, H. Y., Ruby, L. L., Tesfa, T. K., Augusto, G., & Fabrice, P., et al.:](#)

521 [Modeling surface water dynamics in the amazon basin using mosart-inundation](#)
522 [v1.0: impacts of geomorphological parameters and river flow representation.](#)
523 [Geosci. Model. Dev., 10\(3\), 1-42. https://doi.org/10.5194/gmd-10-1233-2017](#),
524 [2017.](#)

525 Mulvaney, T. J.: On the use of self-registering rain and flood gauges in making
526 observations of the relations of rainfall and of flood discharges in a given
527 catchment, in: Proceedings Institution of Civil Engineers, Dublin, Vol. 4, 18–31,
528 1850.

529 Pappenberger, F., Ramos, M. H., Cloke, H. L., Wetterhall, F., Alfieri, L., Bogner, K.,
530 et al.: How do I know if my forecasts are better? Using benchmarks in
531 hydrological ensemble prediction. *J. Hydrol.* 522, 697–713.
532 <https://doi.org/10.1016/j.jhydrol.2015.01.024>, 2015.

533 Parsons, D. B., Beland, M., Burridge, D., Bougeault, P., Brunet, G., Caughey, J., et al.:
534 Thorpex research and the science of prediction. *Bull. Am. Meteorol. Soc.*, 98,
535 807-830, <https://doi.org/10.1175/BAMS-D-14-00025.1> , 2017.

536 Robertson, D. E., Wang, Q. J.: Seasonal Forecasts of Unregulated Inflows into the
537 Murray River, Australia. *Water. Resour. Manag.* 27(8):2747–2769.
538 <https://doi.org/10.1007/s11269-013-0313-4>, 2013.

539 Shao, J., Wang, J., Lv, S., Bing, J.: Spatial and temporal variability of seasonal
540 precipitation in Poyang Lake basin and possible links with climate indices.
541 *Hydrol. Res.* 47(S1):51–68. <https://doi.org/10.2166/nh.2016.249>, 2016.

542 Toth, Z., Zhu, Y., Marchok, T.: The use of ensembles to identify forecasts with small

543 and large uncertainty. *Weather Forecast* 16(4), 463-463.
544 [https://doi.org/10.1175/1520-0434\(2001\)0162.0.CO;2](https://doi.org/10.1175/1520-0434(2001)0162.0.CO;2), 2001.

545 Wang, R., Zhang, J., Guo, E., Zhao, C., Cao, T.: Spatial and temporal variations of
546 precipitation concentration and their relationships with large-scale atmospheric
547 circulations across Northeast China. *Atmos. Res.* 222:62–73.
548 <https://doi.org/10.1016/j.atmosres.2019.02.008>, 2019.

549 Wilks, D. S.: *Statistical Methods in the Atmospheric Sciences*, Volume 91, Second
550 Edition (International Geophysics), 2005.

551 Wood, E. F., et al.: Hyperresolution global land surface modeling: Meeting a grand
552 challenge for monitoring Earth’s terrestrial water. *Water Resour. Res.*, 47,
553 W05301, <https://doi.org/10.1029/2010WR010090>, 2011.

554 Xu, Y.P., Gao, X., Zhang, Y., Kang, L.: Coupling a regional climate model and
555 distributed hydrological model to assess future water resources in Jinhua River
556 Basin, East China. *ASCE. J. Hydrol. Eng.* 20, 2015,
557 [https://doi.org/10.1061/\(ASCE\)HE.1943-5584.0001007](https://doi.org/10.1061/(ASCE)HE.1943-5584.0001007), 2015.

558 Yang, S., Yang, D., Chen, J., Santisirisomboon, J., Zhao, B.: A physical process and
559 machine learning combined hydrological model for daily streamflow
560 simulations of large watersheds with limited observation data. *J. Hydrol.* 590,
561 125206. <https://doi.org/10.1016/j.jhydrol.2020.125206>, 2020.

562 Yaseen, Z.M., Sulaiman, S.O., Deo, R.C., Chau, K.-W.: An enhanced extreme learning
563 machine model for river flow forecasting: State-of-the-art, practical applications
564 in water resource engineering area and future research direction. *J. Hydrol.* 569,

565 387–408. <https://doi.org/10.1016/j.jhydrol.2018.11.069>, 2018.

566 Ye, A., Duan, Q., Yuan, X., Wood, E. F., Schaake, J.: Hydrologic post-processing of
567 MOPEX streamflow simulations. *J. Hydrol.* 508, 147-156,
568 doi:10.1016/j.jhydrol.2013.10.055, 2014

569 Yuan, X., Ma, F., Wang, L., Zheng, Z., Ma, Z., Ye A., Peng, S.: An experimental
570 seasonal hydrological forecasting system over the Yellow River basin-Part 1:
571 Understanding the role of initial hydrological conditions. *Hydrol. Earth Syst. Sci.*
572 20, 2437–2451, <https://doi.org/10.5194/hess-20-2437-2016>, 2016.

573 Yuan, X., S. Wang, and Z.-Z. Hu, 2018a: Do climate change and El Niño increase
574 likelihood of Yangtze River extreme rainfall? *Bull. Am. Meteorol. Soc.* 99,
575 S113-S117, <https://doi.org/10.1175/BAMS-D-17-0089.1>, 2018a.

576 Yuan, X., Ji, P., Wang, L., Liang, X. Z., Yang, K., Ye, A., et al.: High - resolution land
577 surface modeling of hydrological changes over the sanjiangyuan region in the
578 eastern tibetan plateau: 1. model development and evaluation. *J. Adv. Model*
579 *Earth Syst.* <https://doi.org/10.1029/2018MS001412>, 2018b.

580 Zhang, Y., Erkyihum, S. T., Block, P.: Filling the GERD: evaluating hydroclimatic
581 variability and impoundment strategies for Blue Nile riparian countries, *Water*
582 *Int.*, 41, 593–610. <https://doi.org/10.1080/02508060.2016.1178467>, 2016.

583 Zhao, T.T.G., Cai, X.M., Yang, D.W.: Effect of streamflow forecast uncertainty on
584 real-time reservoir operation. *Adv. Water Resour.* 34 (4), 495–504,
585 <https://doi.org/10.1016/j.advwatres.2011.01.004>, 2011.

586 Zhu, E., X. Yuan., A. Wood.: Benchmark Decadal Forecast Skill for Terrestrial Water

587 Storage Estimated by an Elasticity Framework. Nat. Commun. 10, 1237,
588 <https://doi.org/10.1038/s41467-019-09245-3>, 2019.
589

590 **Table 1.** Information of hydrological gauges.

Gauge	Longitude ($^{\circ}$ E)	Latitude ($^{\circ}$ N)	Drainage area (km^2)
Longtan	107.09	25.00	-
Yantan	107.50	24.11	5950 (orange area in Fig. 1)
Luofu	107.36	24.90	800 (green area in Fig. 1)
Jiazhuan	107.12	24.21	2150 (purple area in Fig. 1)

591

592

Table 2. Information of hydrological datasets

<u>Dataset</u>	<u>Time Range</u>	<u>Time step</u>
<u>Rain Gauge Observation Forcing</u>	<u>2013/1/1 ~ 2017/12/31</u>	<u>Hourly</u>
<u>Longtan & Yantan Discharge Gauge</u>	<u>2013/1/1 ~ 2017/12/31</u>	<u>Hourly</u>
<u>Streamflow data</u>		
<u>Jiazhuan & Luofu Discharge Gauge</u>	<u>2013/4/1 ~ 2017/9/30</u>	<u>Daily</u>
<u>Streamflow data</u>		
<u>TIGGE-ECMWF Forecast Forcing</u>	<u>2013/4/1 ~ 2017/9/30</u>	<u>Hourly</u>

593

594

Table 3. Descriptions of calibrated parameters

<u>Parameters</u>	<u>Range</u>
<u>Maximum velocity of baseflow (mm/day)</u>	<u>0.00000116 ~ 0.000579</u>
<u>Fraction of maximum velocity of baseflow where non-linear baseflow begins</u>	<u>0.001 ~ 0.99</u>
<u>Fraction of maximum soil moisture where non-linear baseflow occurs</u>	<u>0.2 ~ 0.99</u>
<u>Variable infiltration curve parameter</u>	<u>0.001 ~ 1</u>
<u>River width (m)</u>	<u>0 ~ 101.16</u>
<u>River depth (m)</u>	<u>0 ~ 6.46</u>
<u>River density (km/km²)</u>	<u>0.049 ~ 1.03</u>
<u>River roughness</u>	<u>0.033 ~ 0.05</u>
<u>River slope</u>	<u>0.015 ~ 0.47</u>

595

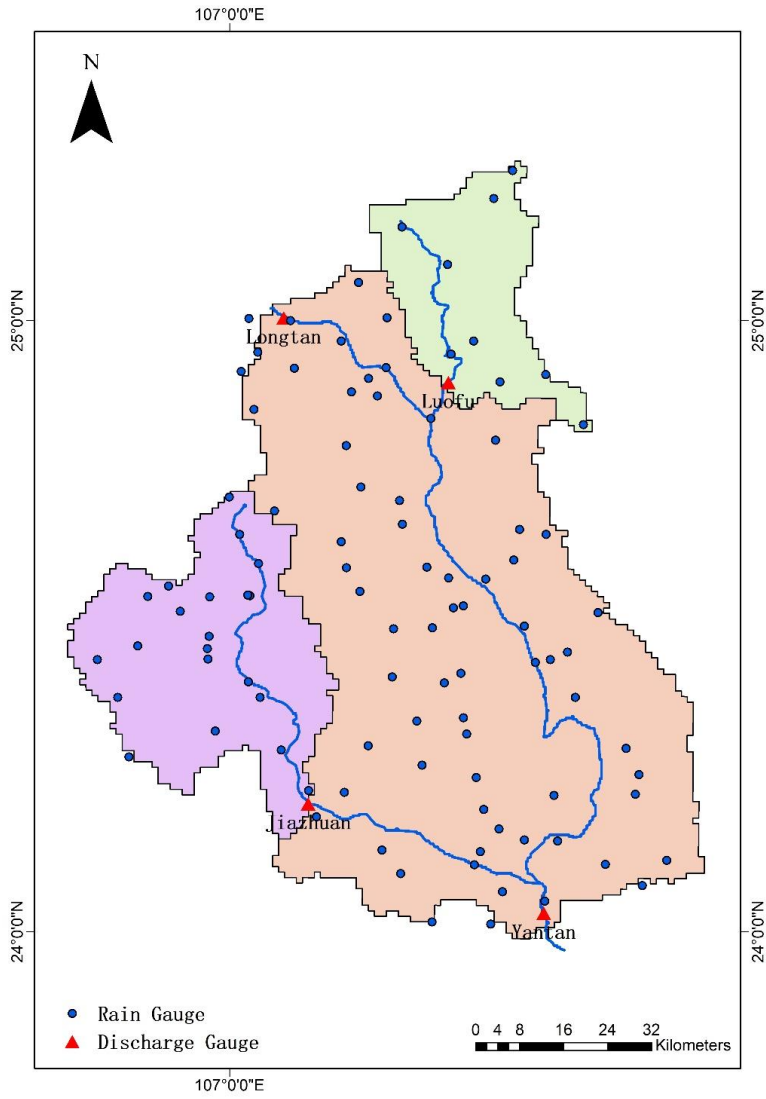
带格式的：两端对齐，行距：2 倍
行距，无孤行控制

596

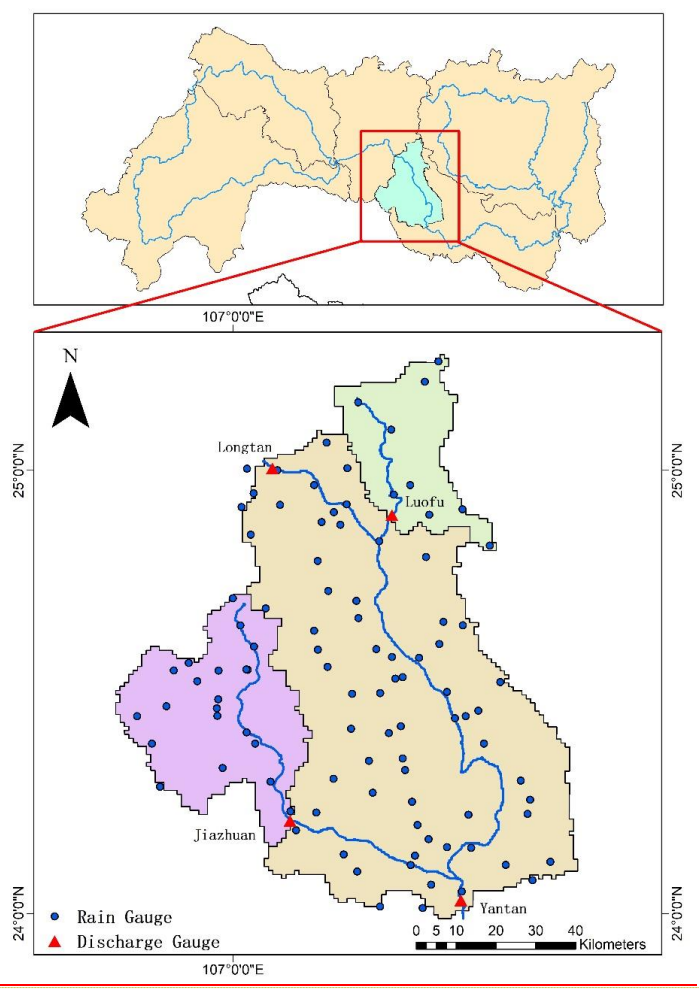
Table 42. Experimental design in this study.

Experiments	Description
ESP-Hydro	Using CSSPv2 land surface hydrological model driven by randomly-sampled historical meteorological forcings
Meteo-Hydro	Using CSSPv2 model driven by bias-corrected TIGGE-ECMWF hindcast meteorological forcings
Meteo-Hydro-LSTM	Using LSTM model to correct streamflow from Meteo-Hydro hindcast
LSTM	Using LSTM model to forecast streamflow based on observation only

597



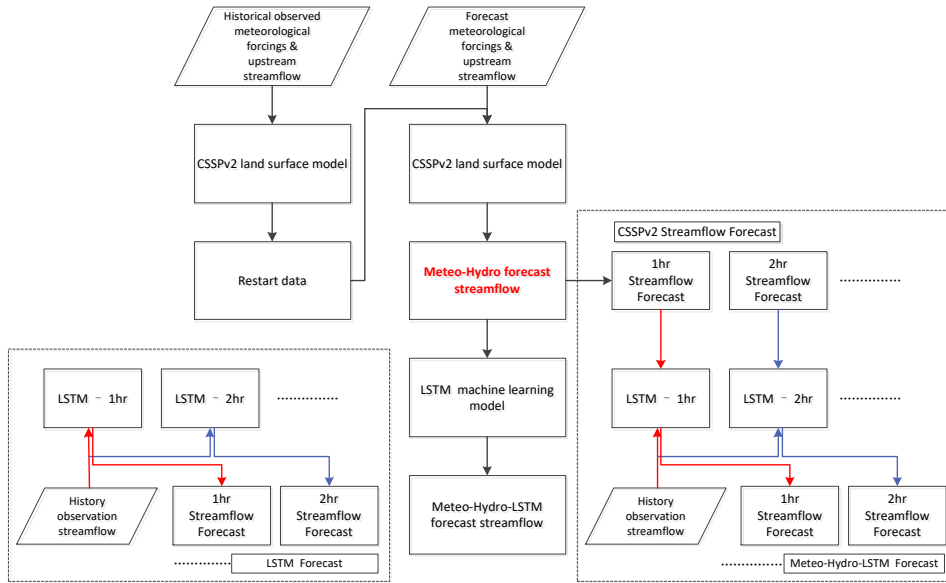
带格式的: 字体: (中文) + 中文正
文 (等线), 小四



600

601 **Figure 1.** Locations of discharge gauges and rain gauges over the Yantan basin.

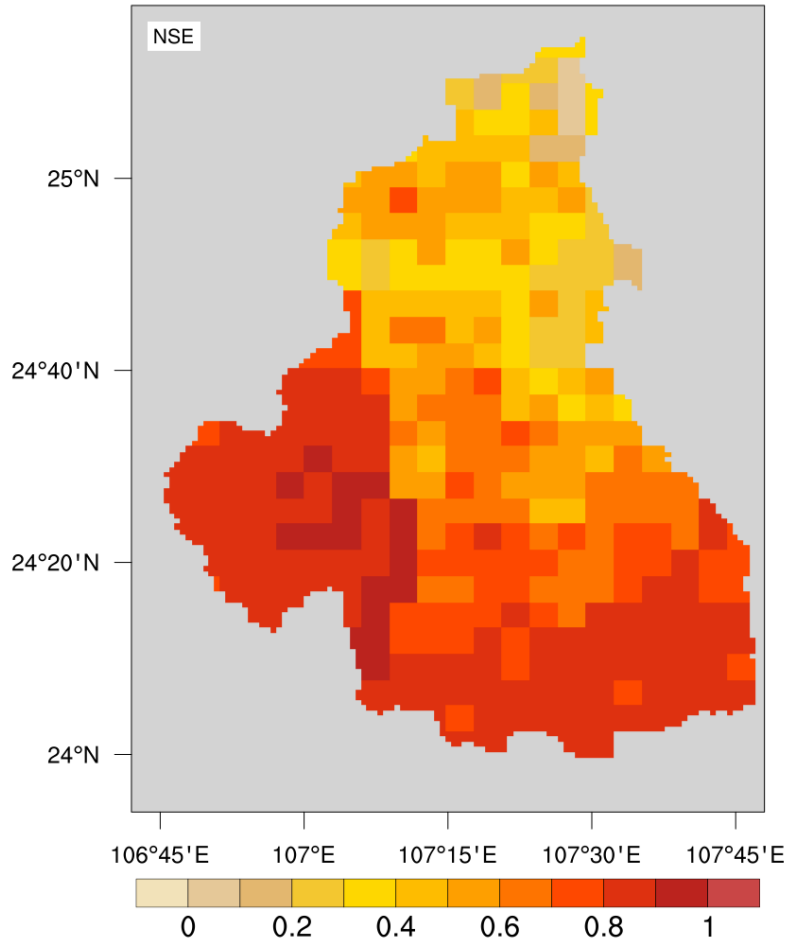
602



603

604 **Figure 2.** A diagram for the integrated hydrometeorological and machine learning
605 streamflow prediction.

606



607

608 **Figure 3.** Nash-Sutcliffe efficiency coefficients for the calibrated grid runoff simulation

609 from CSSPv2.

610

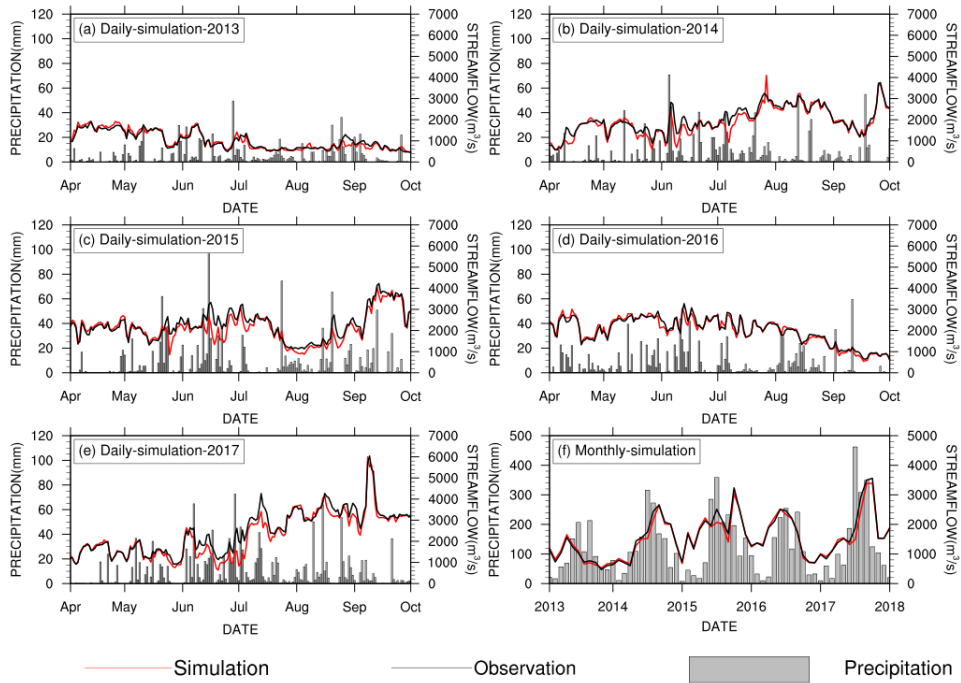
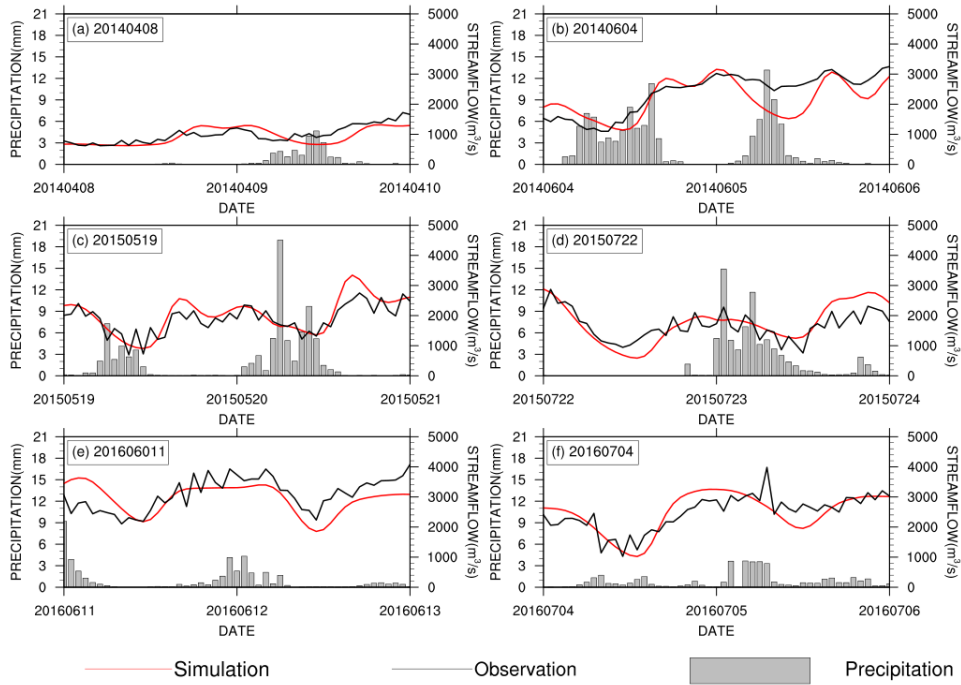


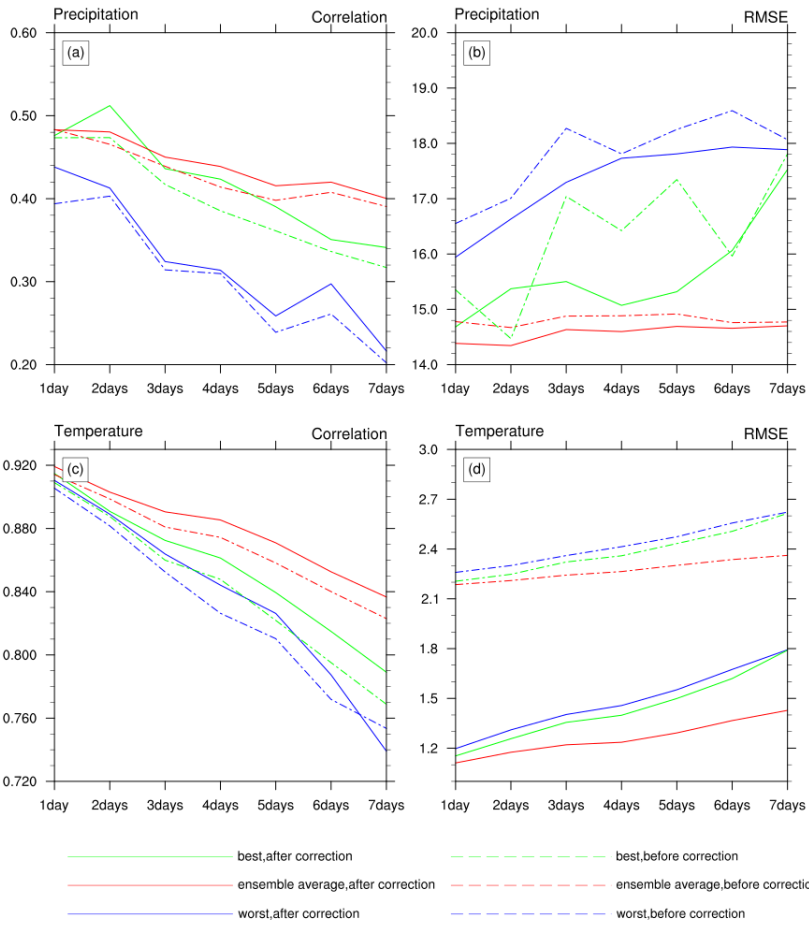
Figure 4. Evaluation of streamflow simulations at Yantan gauge. The black and red lines are observed and simulated streamflow. (a)-(e) are for daily streamflow, and (f) is for monthly streamflow. The gray bars represent daily (or monthly) precipitation.

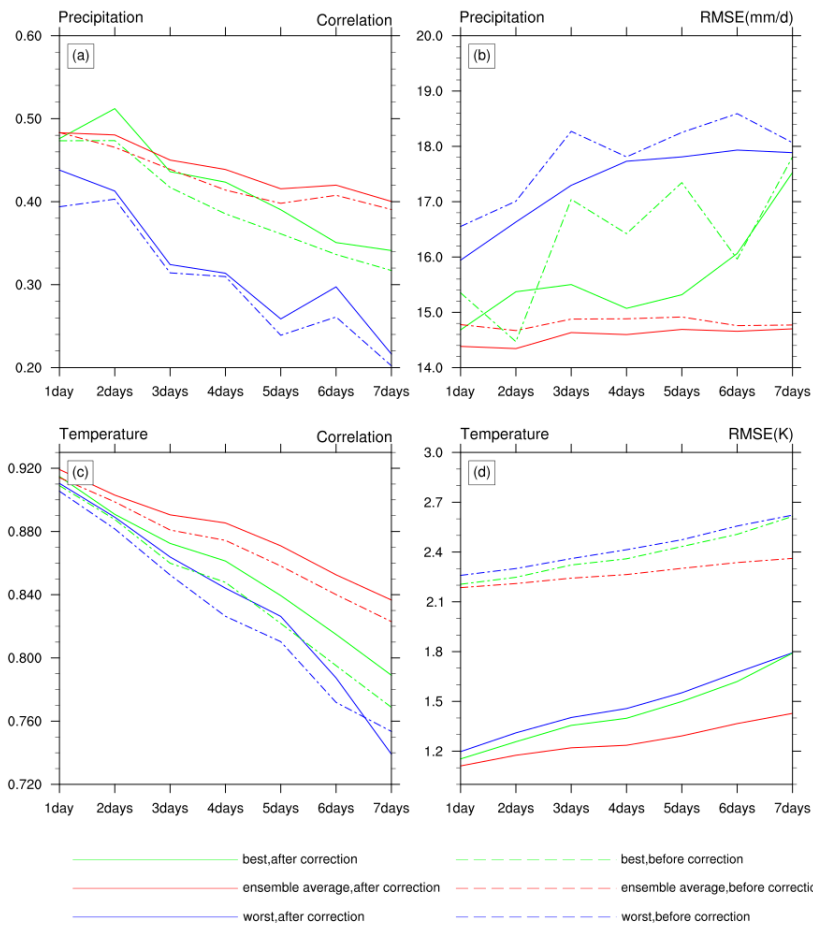
615



616

617 **Figure 5.** The same as Figure 4, but for the evaluation of hourly streamflow
618 simulations at Yantan gauge.



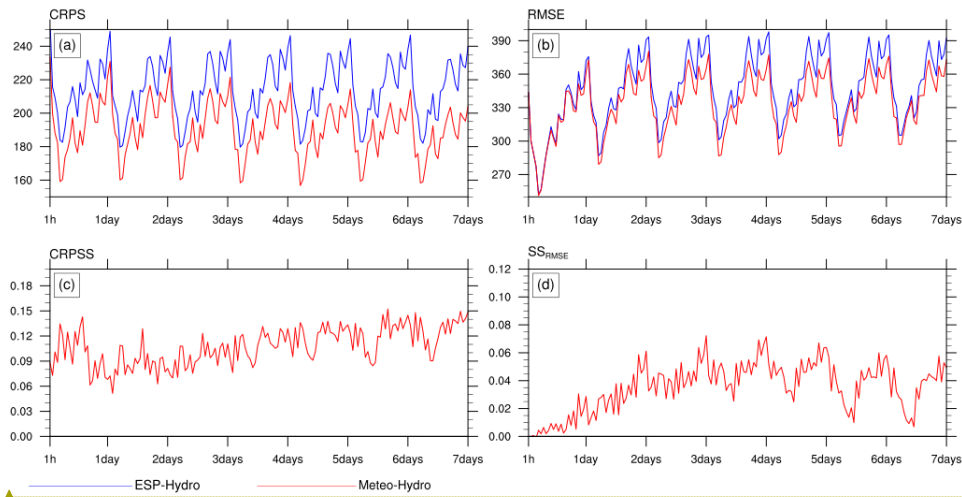


带格式的: 字体: (中文) + 中文正文 (等线), 小四

621

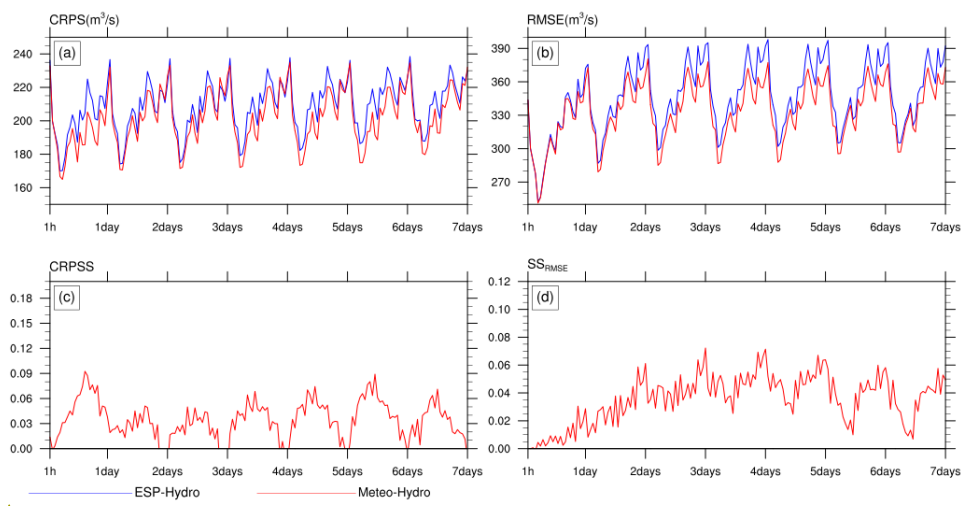
622 **Figure 6.** Evaluation of precipitation and temperature hindcasts from
 623 TIGGE-ECMWF. The red and blue lines represent the best and worst results among 51
 624 TIGGE-ECMWF ensemble members respectively, and the green lines represent the
 625 results for the ensemble means of 51 members. Solid and dashed lines represent the
 626 results after and before bias corrections, respectively.

627



628

带格式的: 字体: (中文) + 中文正文 (等线), 小四

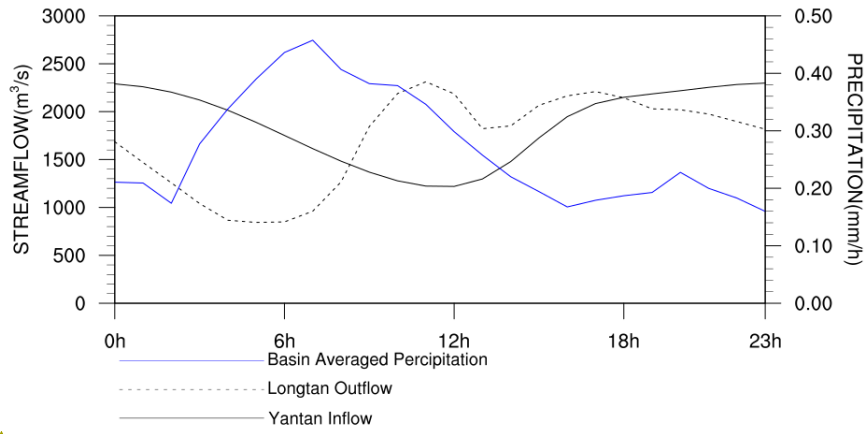


629

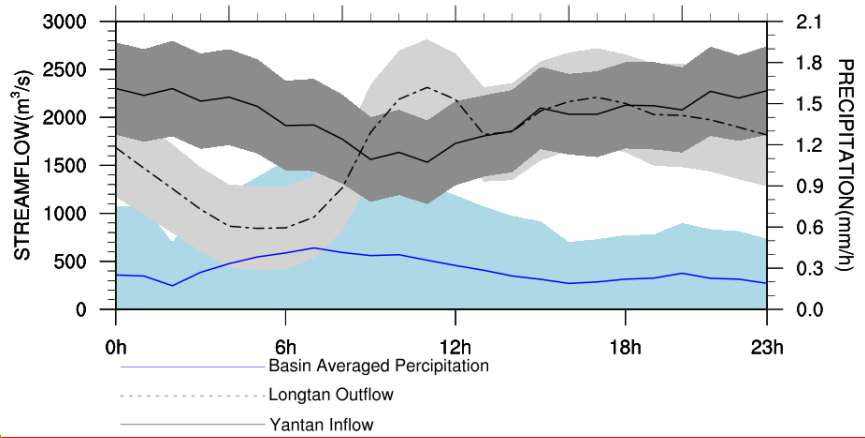
带格式的: 字体: (中文) + 中文正文 (等线), 小四

630 **Figure 7.** (a) Continuous Ranked Probability Score (CRPS) and (b) Root Mean
631 Squared Error (RMSE) for daily streamflow ensemble forecasts at Yantan gauge. (c)
632 and (d) are the skill score in terms of CRPS and RMSE for Meteo+Hydro, where
633 ESP+Hydro is used as reference forecast.

634



635



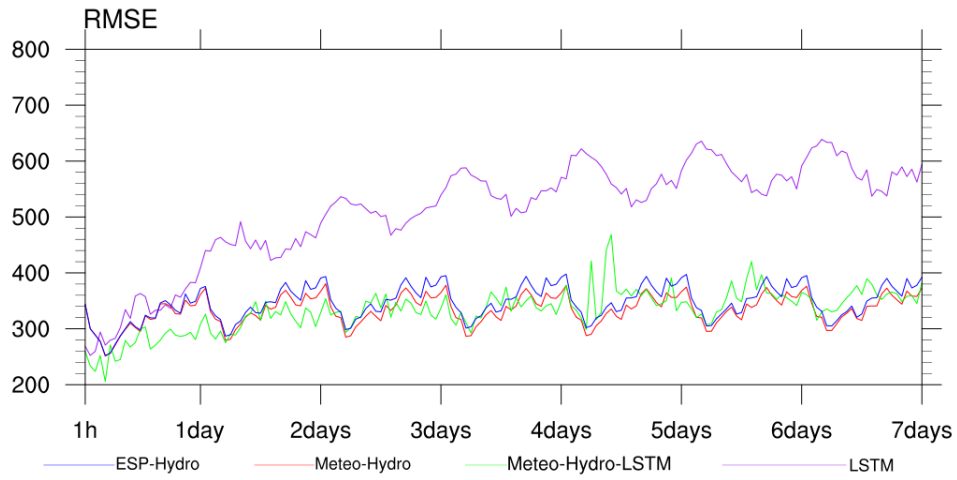
636

637 **Figure 8.** Diurnal cycle of Longtan outflow (m^3/s ; dashed black line), Yantan inflow
638 (m^3/s ; solid black line) and basin-averaged precipitation (mm/h ; blue line).

带格式的: 字体: (中文) + 中文正文 (等线), 小四

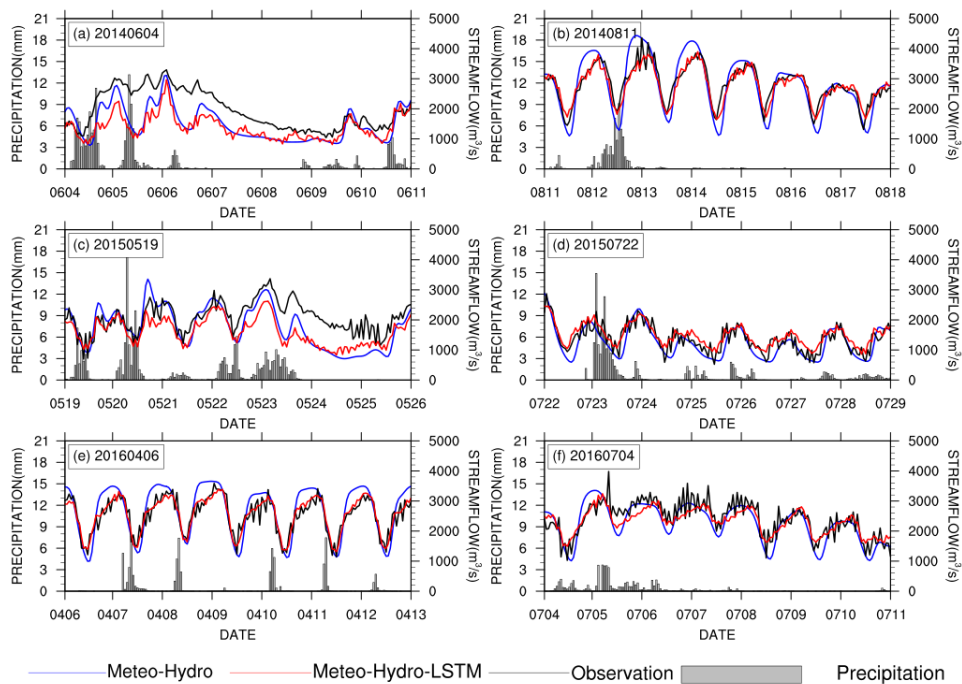
带格式的: 字体: (中文) + 中文正文 (等线), 小四

639



640

641 **Figure 9.** RMSE (m^3/s) for hourly streamflow hindcasts from four forecast
642 approaches. The green line represents the Meteo+Hydro+LSTM forecast, the red line
643 represents the Meteo+Hydro forecast, the blue line represent the ESP+Hydro forecast,
644 and the purple line represents the LSTM forecast based on historical streamflow
645 observation alone.



646

647 **Figure 10.** Evaluation of the forecast approaches for a few flooding events. The black
 648 lines are observed streamflow from Yantan hydrological gauge, the blue lines are the
 649 Meteo+Hydro ensemble mean streamflow forecast, and the red lines are the
 650 Meteo+Hydro+LSTM forecast streamflow by using Meteo+Hydro ensemble mean
 651 forecast with LSTM. The gray bars represent hourly precipitation averaged over the
 652 basin.